Seismic performance of bridges during the 2016 Central Italy earthquakes

Di Sarno L., da Porto, F. , Guerrini, G., Calvi, P.M., Camata, G. and Prota, A.

ABSTRACT

This paper focuses on the structural performance of existing masonry and reinforced concrete bridges which were surveyed in the aftermath of the 2016 Central Italy earthquakes. Typical bridge vulnerabilities are first reviewed, as they provide a reference for the response of the bridges that were damaged by the 2016 earthquake swarm. Case studies are then discussed and preliminary numerical analyses are carried out to interpret the observed failure modes. In general, all surveyed masonry bridges experienced some extent of damage, particularly when built with poor-quality materials and subjected to geotechnical-induced effects. However, they offered a robust response in terms of collapse prevention. The majority of existing reinforced concrete bridges, although designed primarily for gravity loads, exhibited acceptable performance; however, local damage due to the poor maintenance of the structural systems was observed, which affected primarily the non-structural components of the bridges.

1 INTRODUCTION

Three major earthquake events occurred in Central Italy in 2016. The first event, with magnitude M6.1, took place on August 24, the second one (M5.9) on October 26, and the third one (M6.5) on October 30. Each event was followed by many aftershocks [1, 2]. The August-October 2016 earthquake sequence occurred on mapped normal faults in the Apennine Mountain range in central Italy, a region with a long history of destructive earthquakes. Nevertheless, widespread damage was caused by the 2016 seismic sequence to the built environment. Several collapses of masonry and reinforced concrete (RC) residential buildings were recorded, since most buildings were designed primarily for gravity loads and did not possess adequate lateral stiffness, strength, or ductile detailing. Lifelines, especially roadways, were also severely damaged, with consequences for the rescue operations as the access to the affected areas became limited and alternative routes were not efficient. Furthermore, transportation systems are expected to possess high resilience in the aftermath of extreme events, such as earthquakes and floods, to allow easy access to local communities. However, it has been found that the existing bridge infrastructures, especially in South of Europe, exhibit high vulnerability [3, 4, 5, 6] and risk mitigation policies are deemed urgent. Additionally, recent studies have shown that current assessment methods for existing RC bridge structures need to be further investigated as they tend to provide unrealistic estimations for brittle failure modes [7, 8], especially for non-ductile systems under multiple earthquake records (e.g. [9], among others).

This paper illustrates the structural performance of existing masonry and RC bridges which were surveyed in the aftermath of the 2016 Central Italy seismic sequence. The paper provides an outline of the typical bridge vulnerabilities, as observed during past earthquakes, and focuses on the response of the bridges either damaged or partially collapsed after the 2016 earthquake swarm. Case studies are considered and preliminary numerical analyses are carried out to interpret the observed damage. It was found that structural damage was widespread in masonry structural systems, which in general were characterized by very low-quality materials and were also primarily affected by geotechnical induced effects. RC bridges showed acceptable performance: the limited damage occurrence, localized particularly in RC decks, was mostly attributed to the poor maintenance of the structural systems. Thus, poor quality of construction materials, aging phenomena, and scarce maintenance can significantly increase the vulnerability of existing structures subjected to seismic loads.

2 SEISMIC PERFORMANCE OF BRIDGES DURING PAST EARTHQUAKES

2.1 Masonry bridges

Masonry arch bridges are usually quite robust structural systems [10], as demonstrated by on-site surveys carried out during past seismic emergencies: in many circumstances they withstood major earthquakes with no or limited damage. This has been reported starting from the Irpinia, Italy earthquake of 1980 [11] up to the recent 2008 earthquakes of Wenchuan, China [12, 13]. After the L'Aquila, Italy earthquake of 2009, the one-track railway line from Rome to Sulmona, which includes several multi-span arch masonry bridges, was fully reopened 3 days after the main shock [14].

The main damage and collapse mechanisms reported from past earthquakes, validated on the basis of experimental and numerical analyses, consist of local and overall collapses in the longitudinal and transverse directions. These mechanisms develop in relation to the main geometrical features of the masonry arch bridges, such as number of spans, span length, arch rise, arch ring thickness, abutment (for single-span) or pier (for multi-span bridges) height, transverse bridge width, among the most relevant ones.

Single-span masonry arch bridges generally have massive abutments, which in most cases can be represented by infinitely rigid constraints. In this configuration, a local arch mechanism can be triggered in the longitudinal direction (mechanism A-L) under seismic action. This is an asymmetric collapse mechanism with the formation of three rigid voussoirs and four hinges (Fig. 1a), located where the thrust line (red line in the figure) crosses the arch ring boundaries [15]; the input accelerations activating this local mechanism are lower for semi-circular arches than for segmental arches [16, 17]. In the case of single-span structures with more slender abutments an overall arch-abutment longitudinal mechanism may develop (mechanism AA-L), with hinges at the base of the abutments and in the arch (e.g. [18] among others) as shown in Figure 1b. This overall arch-abutment longitudinal mechanism is generally more vulnerable than the local arch mechanism typical of squat single-span bridges [16, 17].

In squat multi-span bridges, the spandrel walls at the arch springing provide fixed restraints for the arch, so that each span can be regarded as independent. The expected collapse mechanisms are the same as those for single-span bridges with squat abutments, i.e. mechanism A-L, for any individual arch in the longitudinal direction. Conversely, in multi-span structures with slender piers, the kinematic chain in the longitudinal direction may either involve the arches alone, or an overall arch-pier longitudinal mechanism may develop (mechanism AP-L, Figure 2a), with the formation of plastic hinges at the pier bases and in the arches. Local A-L and overall AP-L collapse mechanisms are both possible for multi-span arch bridges with piers of medium slenderness (pier height-to-depth ratio between 1 and 4). An example of damage due to large displacement of the bridge in the longitudinal direction can be found in the Guantong Bridge, China, an unreinforced sandstone masonry arch bridge hit by the 2008 Wenchuan earthquake (Figures 2b and 2c).

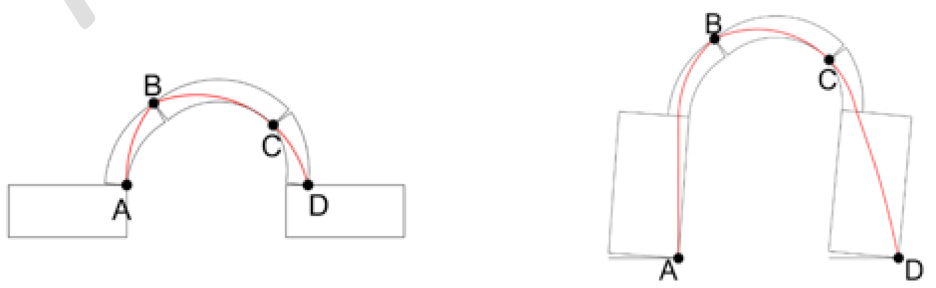

(a) (b)

Figure 1 - Single-span bridges: (a) local longitudinal arch mechanism (A-L) and (b) overall longitudinal arch-abutment mechanism (AA-L).

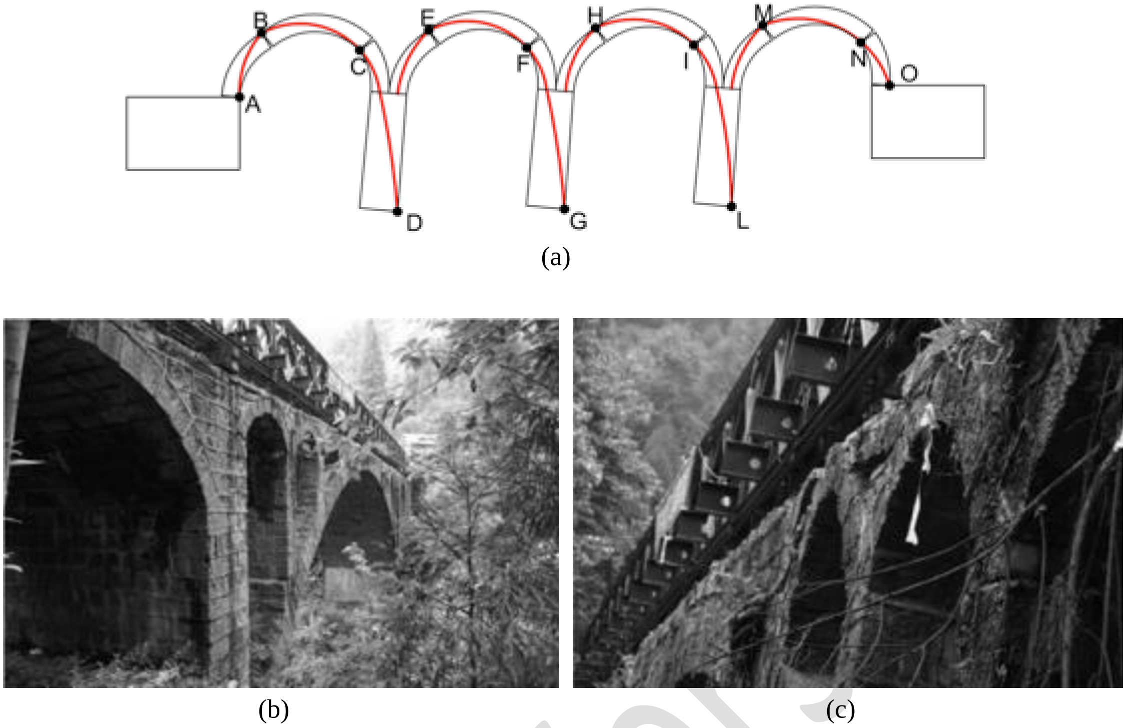

Figure 2 - Multi-span bridges: (a) overall longitudinal arch-pier mechanism (AP-L); (b, c) damage to the Guantong Bridge, China, due to large displacements in the longitudinal direction in the 2008 Wenchuan earthquake (after [13]).

Considering the response in the transverse direction, spandrel walls are often the most vulnerable elements and may easily rotate out-of-plane in a spandrel-wall transverse mechanism (mechanism SW-T, Figure 3a). Damage or overturning of these secondary elements does not generally jeopardize the overall structural safety of the bridge. However, subsequent loss of infill material may compromise road pavement support and hence bridge functionality. These local collapse mechanisms are usually related to the lowest limit accelerations and simple retrofit to prevent spandrel overturning can be very effective [16]. Other local out-of-plane failures involve abutment wing walls and parapets. Examples of overturning of spandrel walls (Figure 3b), spandrel walls and parapets (Figure 3c), and wing walls and parapets (Figure 3d) have been often reported in recent earthquakes.

In multi-span bridges with slender piers an overall collapse mechanism can occur in the transverse direction involving both arches and piers (AP-T): flexural hinges can form at the pier bases, due to bending in a vertical plane, and at the arch crowns, due to bending in a horizontal plane [22] (Figure 4a). A global collapse of this type was reported for the Yingchun Bridge (Figure 4b), which failed because the arch supports lost stability and the retaining walls at the supports toppled outward in the 2008 Wenchuan earthquake in China. Another example is the collapse of the slender multi-span bridge spanning the Río Claro in the 2010 Maule earthquake in Chile (Figures 4c and 4d). Multi-span arch bridges with slender piers are generally more vulnerable to overall collapse mechanisms in both longitudinal and transverse directions (AP-L and AP-T), than to local longitudinal arch mechanisms (A-L). However, for common bridge geometries, the limit accelerations associated with these mechanisms are rather high [16, 17] compared to those triggering local spandrel mechanisms (SW-T).

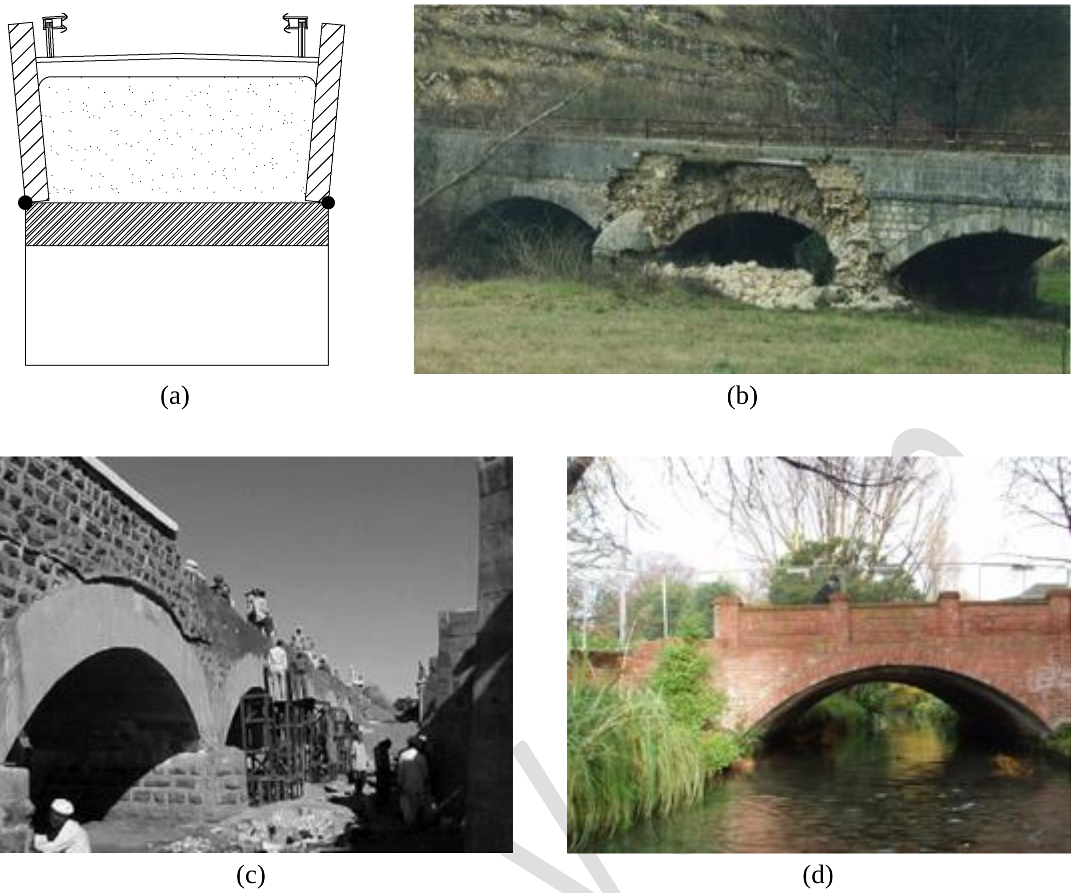

Figure 3 - Local transverse mechanisms: (a) out-of-plane overturning of spandrel wall (SW-T); (b) out-of-plane collapse of a spandrel wall in the 1997 Umbria and Marche earthquake, Italy (after [19]); (c) damage to a railway masonry arch bridge in the 2001 Bhuj earthquake, India (after [20]); (d) collapse of wing wall and parapet of the Kahu Road East Bridge in the 2011 New Zealand earthquake (after [21]).

Most of the aforementioned mechanisms are based on the assumption of infinitely stiff and strong abutments and foundations. However, local failures of the abutments (flexural failure, AB_NM; and shear failure, AB_S) and of the abutment-foundation interface (sliding, AB_SL; and overturning, AB_OV), may also occur. Soil-structure interaction and foundation settlements can cause significant damage, as masonry arch bridges are extremely stiff structures: hence, widespread significant damage can be observed in case of differential settlements of the supports. Moreover, the load-bearing capacity of masonry bridges can be affected by the local attainment of strength, typically when poor materials such as low-quality mortar were used in construction. In stone masonry bridge structures, with piers or abutments characterized by filling with discontinuities, cavities, and/or loose material, local effects of disaggregation of masonry units and loss of support can be observed also under low inertial forces.
Aging and deterioration of material strength may also have an impact on the seismic behavior of masonry bridges. Most of these structures are part of the historical heritage of the 19th century, while some date back to the Renaissance or the Roman Era; nevertheless they are still in service. Due to their long life, the effects of natural weathering, aging, and increased traffic can be significant [24]. Deterioration conditions such as erosion of mortar joints, salt efflorescence in bricks, arch barrel deformations with cracking, separation between masonry rings in multi-barrel vaults, sliding, and bulging or detachment of spandrel walls, are often observed in in-service masonry bridges, with the potential of reducing the seismic capacity of the structure.

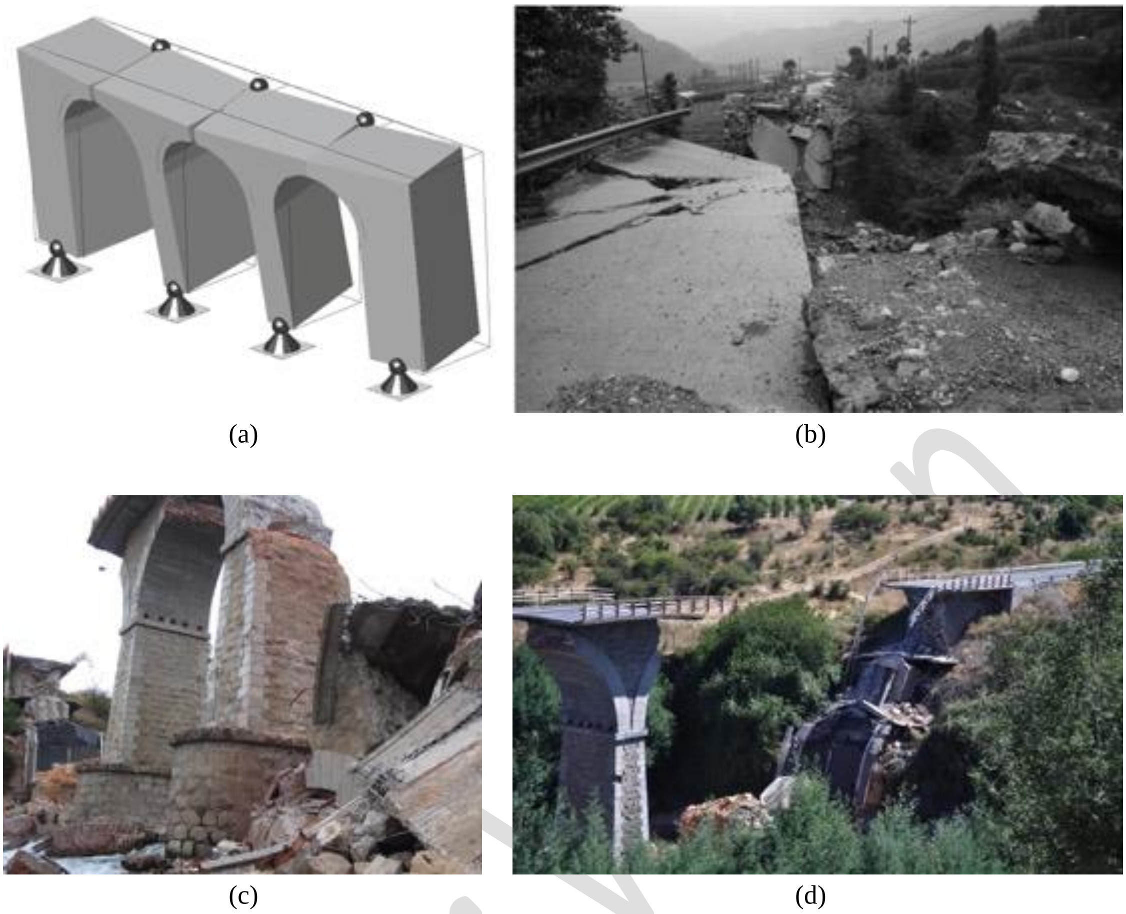

Figure 4 - Overall transverse mechanisms: (a) overall AP-T mechanism of multi-span bridges; (b) collapse of the Yingchun Bridge in the 2008 Wenchuan earthquake, China (after [13]); (c, d): collapse of the Río Claro Bridge in the 2010 Maule earthquake, Chile (after [23]).

2.2 Reinforced concrete bridges

The causes of failure in RC bridges are many and difficult to categorize. However, most damage and collapse cases in recent worldwide earthquakes fall into the following categories: substructure, superstructure, soil-structure interaction, and nonstructural damage.

As primary components of the gravity and lateral force-resisting system of bridges, piers are subjected to intense forces during earthquakes. Damage to piers depends largely on bridge geometry, structural design and seismic details, if any. Short, stout piers are more susceptible to shear failure. Lack of specific design details, such as insufficient reinforcement lap length or inadequate transverse reinforcement, can lead to premature failure, as surveyed for example in the aftermath of the 1994 Northridge (California) and 1995 Kobe (Japan) earthquakes (Figure 5). Additionally, because of flexure-torsion interaction, many RC bridge piers of curved and skewed bridges suffered severe damages during the 2008 Wenchuan earthquake in China [12, 25].

High shear demands typically develop within joints between piers and superstructure. The heavy damage observed on several RC bridges in the San Francisco Bay Area during the 1989 Loma Prieta earthquake dramatically highlighted this problem (Figure 6). Current design philosophies aim at capacity designing these connections in order to force inelastic actions to occur in beams and columns. Without adequate transverse reinforcement, concrete diagonal cracks occur in the joint regions, because of excessive shear-induced tensile stresses (Figure 6). Moreover, beam longitudinal bars do not anchor properly if bent within poorly confined joints, with the risk of bond failure.

(a) (b)

Figure 5 - Typical failure of bridge piers: (a) confinement failure at a bridge pier top during the 1994 Northridge earthquake (courtesy of NISEE) and (b) flexural failure above base of columns of the Hanshin expressway, due to premature termination of longitudinal reinforcement and inadequate confinement in the 1995 Kobe earthquake: overall collapse (top) and close-up view of the failure mechanism (courtesy of Kawashima).

Figure 6 - Shear failure of pier-bent cap joints, and anchorage failure of beam longitudinal bars of the Cypress viaduct in Oakland, California, during the 1989 Loma Prieta earthquake (courtesy of NISEE).

Bearings are designed to transfer forces and allow relative motion between superstructure and substructure elements. Damage to bearings during earthquakes varies by bearing type: some examples include sliding of elastomeric bearings and pull-out or shearing of anchor bolts. Failure of bearings can contribute to unseating of spans, which occurs when the bridge superstructure is permanently displaced from its position atop the substructure. Some older bridges have very short bearing seat lengths, which makes unseating far more likely. Unseating can involve girders displacing from their bearings and coming to rest on the pier cap, but can also result in the complete collapse of one or more spans.

Expansion joints are designed to allow relative motion between superstructure segments due to temperature fluctuations, creep, shrinkage, and traffic loads. However, earthquakes can cause sudden closing or opening of expansion joints, which may cause concrete crushing or span discontinuities, respectively. Pounding between adjacent girders is also often observed when the ground motion imposes large relative displacements to the piers or to the portal frames supporting the bridge deck.

Abutment behavior is affected not only by the response of its structural components, but also by the interaction with the surrounding soil. Abutments typically consist of bearings, wing walls, back walls, and foundation elements. Abutments often include shear keys, which aid in restraining the relative motion between the superstructure and the abutment itself, and can act as structural fuses whose failure limits damage to other elements of the structure. Pounding may also occur between the bridge deck and the abutments.

Nonstructural elements include railings, barriers, signage, and utility conduits. Damage to these elements does not affect the structural integrity of the bridge, but secondary effects such as injuries can occur as a result of their failure. Examples include impact damage from falling overhead signs, risk of electrocution of passersby by severed electrical wires, and damaged barriers failing to prevent roadway departures.

In recent Italian earthquakes such as the 2009 L'Aquila earthquake and the 2012 Emilia earthquake, damage to reinforced concrete bridges was limited, even for those not specifically designed for earthquake resistance (e.g. [26, 27], among many others). In most instances, the observed minor damage was mainly the result of poor maintenance. To this end, the most affected elements were drainage systems and deck bearings. However, movement of the bearings and pounding of bridge deck segments were sometimes reported.

Highways A24 and A25 are two major infrastructures that connect the East coast with the West coast of Italy, and run through the area affected by the 2009 L'Aquila earthquake. The double carriageway bridge decks consist mostly of simply supported, single-span, precast pre-stressed elements, resting on bearings on top of RC piers, as shown in Figure 7 for the "Della Valle" bridge along A24. Bearings and gaps were designed to allow deck thermal deformations and were not conceived to resist horizontal and vertical seismic loads or displacements: many of these supports were unbolted and they could resist lateral loads relying solely on friction. These highways were closed for inspection in the aftermath of the 2009 L'Aquila earthquake and reopened a few days later: no structural damage to the bridges was generally observed, but some interventions were needed to repair the damage induced by pounding, movement or failure of the bearings. Due to lack of internal connections, each segment and each pier behaved independently during the seismic event, causing relative displacements between the deck segments and their supports.

Only a 35-m-long multi-span RC bridge collapsed along a secondary road near the town of Fossa (Figure 8a). The collapse was probably caused by pier failure due to lack of maintenance [26]: the steel reinforcing bars were protected by a thin concrete cover and appeared to be severely corroded. Another 3-span RC bridge, close to the town of Onna (Figure 8b), suffered some damage at the top of the piers: again, damage was mainly due to poor maintenance.

(a) (b)

Figure 7 - "Della Valle" bridge along Highway A24, Italy: (a) bridge configuration; (b) typical damage due to lack of maintenance.

(a) (b)

Figure 8 - Bridge damage in the 2009 L'Aquila earthquake, Italy: (a) bridge collapse near Fossa; (b) deck failure near Onna (after [26]).

In the 2012 Emilia earthquake, Italy, RC bridges sustained only minimal damage [27]. Immediately after the event, inspections indicated some damage located near the expansion joints (mainly cracking) and highlighted maintenance issues, in particular corrosion and drainage deficiencies.

3 BRIDGE PERFORMANCE IN THE AFTERMATH OF THE 2016 CENTRAL ITALY EARTHQUAKES

3.1 Earthquake sequence and inspected bridges

Visual inspections in the area struck by the 2016 Central Italy earthquakes included several bridges and viaducts, in particular:

- "Tre Occhi" bridge, a three-span masonry arch bridge located along the SR260 route in Amatrice (Figure 10);
- "Cinque Occhi" bridge, a five-span masonry arch bridge located along the local road connecting SS4 (Casale Nibbi exit) and SR260 routes, towards Amatrice (Figure 11);
- Two masonry arch bridges along the SP129 "Trisungo-Tufo" route, located near the town of Tufo (Figures 12 and 13);
- "Rosa" bridge, a five-span reinforced concrete deck and girder bridge with masonry piers and abutments (Figure 14);
- Some reinforced concrete viaducts along the SS685 and SS4 state routes, including the "Scandarello" viaduct (Figure 16).

Figure 9 shows the geographic location of the bridges along with the nearest seismic stations belonging to the Italian Accelerometric Network (RAN), managed by the Department of Civil Protection (DPC), and to the Italian Seismic Network, managed by the National Institute of Geology and Volcanology (INGV), which were used to derive the input ground motions for the bridges under examination. A data search was carried out on the closest strong-motion stations for the events of 24/08/2016 and 30/10/2016. The data have been obtained through the ESM portal (Engineering Strong Motion Database, version 1.0; [28]) and are reported in Table 1. The highest values of peak ground acceleration (PGA) were recorded along the East-West direction at all considered stations during both the 24/08/2016 Amatrice earthquake and the 30/10/2016 Norcia earthquake. The vertical component of the seismic action was also significant, with accelerations of the order of 25% to 50% of the horizontal PGA during the first event, and even up to 130% of the horizontal PGA during the second event. It should be noted that the T1214 and T1244 recording stations were installed only after the 24/08/2016 mainshock and that the ACC records of that event were of dubious quality: as a consequence there are no records of the 24/08/2016 earthquake from these stations.

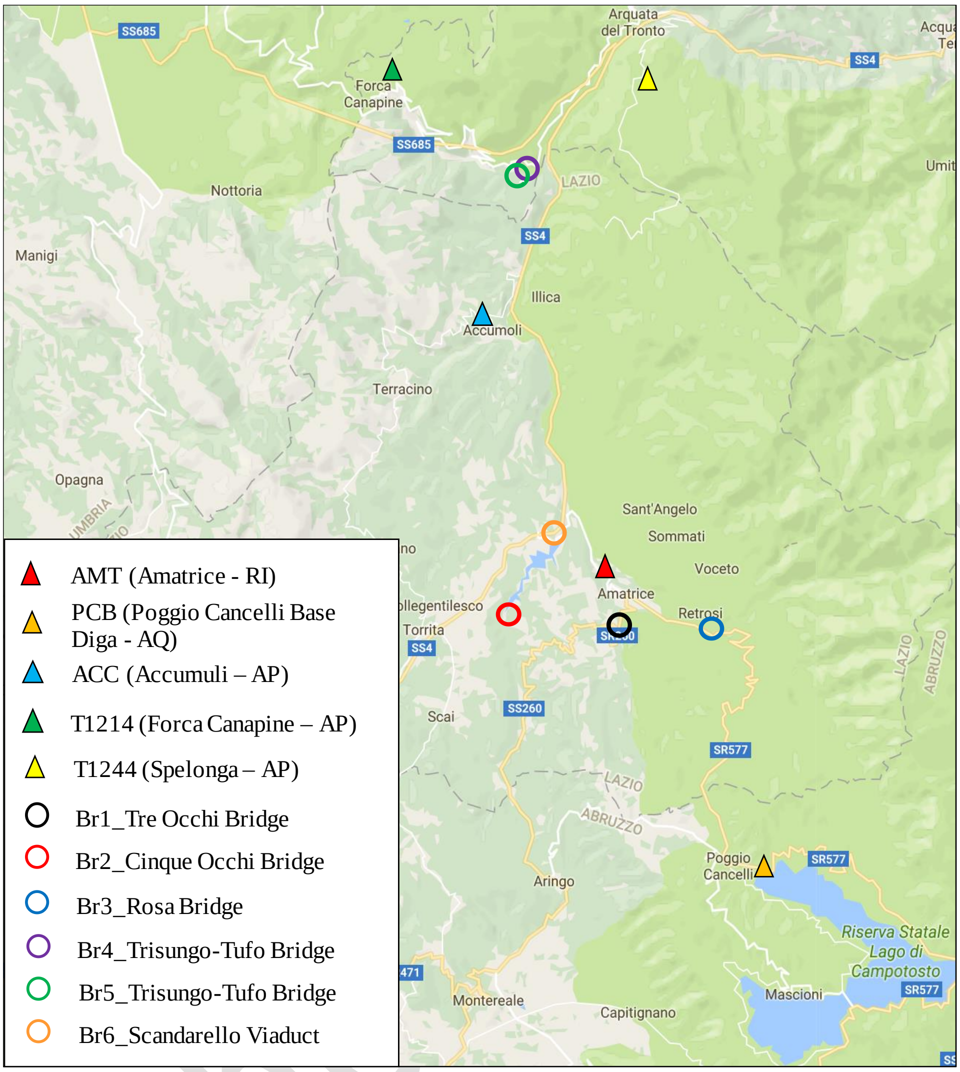

Figure 9 - Location of the inspected bridges and of the nearest seismic stations.

Table 1 - Case-study bridge orientations and seismic data from the closest recording stations.

Bridge	Deck orientation	Recording station	Coordinates	PGA 24/08/2016 [g]			PGA 30/10/2016 [g]		
				N-S	E-W	Vert.	N-S	E-W	Vert.
Tre Occhi	E-W	AMT (Amatrice - RI)	42.63246 N 13.28618 E	0.380	0.870	0.400	0.401	0.532	0.324
Cinque Occhi	NWW-SEE	PCB (Poggio Cancelli Base Diga - AQ)	42.55861 N 13.33799 E	0.189	0.308	0.081	0.244	0.142	0.070
Rosa	NNE-SSW	ACC (Accumoli - AP)	42.69599 N 13.24200 E	-	-	-	0.392	0.434	0.558
Scandarello	NEE-SWW	T1214 (Forca Canapine - AP)	42.75954 N 13.20870 E	-	-	-	0.421	0.604	0.645
Trisungo-Tufo, single span	NEE-SWW	T1244 (Spelonga - AP)	42.75697 N 13.29779 E	-	-	-	0.193	0.285	0.354
Trisungo-Tufo, three spans	Curved								

3.2 Masonry bridges

Figure 10 shows the three-span arch masonry bridge referred to as the “Tre Occhi” bridge in Amatrice, a critical lifeline for access to the town. In the aftermath of the August 24 event it was closed to traffic, and a temporary by-pass road was promptly constructed to re-establish connections to Amatrice from the South. The “Tre Occhi” bridge longitudinal axis is oriented along the East-West direction, which was subjected to the maximum PGA of 0.87 g, during the main event on August 24. The transverse direction was subjected to PGA values equal of 0.38 g and 0.40 g, during the events of August 24 and October 30, respectively.

The semi-circular arch barrels are approximately 5-m-wide, with spans of 12 m. The total width of the deck is about 10 m, as a result of a quite recent widening intervention, with two RC cantilever slabs spanning more than 2.0 m on each side of the barrel vaults. The arches are made of solid bricks, whereas spandrels, abutments and central piers are made of stone masonry. The spandrel walls and abutment wing walls are made of 15- to 300-mm size stones with mortar layers. The piers and the abutments have an external leaf consisting of 450- to 550-mm size, regular-shaped stones with mortar joints; the internal core is made of relatively irregular smaller stones and cobbles, bound with very poor earthen mortar stabilized with a low amount of lime.

Steel ties are provided through the spandrel walls and a few portions of the wing walls (Figures 10a and 10b), as a measure to prevent out-of-plane collapse. Three plain concrete buttresses are built along the North-East wing wall (Figure 10c), while the pier and the abutment toes on the river bed are capped by reinforced concrete walls (Figures 10f and 10g), unlikely part of the original structure.

During the earthquakes, several sections of the external stone masonry layers collapsed out of plane. This occurred particularly in some areas of the abutment walls (Figures 10b and 10c), where ties were not placed. Moreover, wide horizontal cracks opened across the construction cold joints in the buttresses retaining the North-East wing wall (Figure 10c), with residual widths of the order of 10 mm. In addition, sliding occurred along these cracks, with permanent displacements ranging from 10 to 50 mm.

This resulted in a lack of confinement of the interior uncemented cobbles and infill material, causing lateral relaxation and settlement that was visible on the roadway surface above the abutment (Figure 10d): major longitudinal and transverse cracks were observed along the road surface, with maximum widths of about 60 mm vertically and 30 mm horizontally. A widespread deformation pattern had already developed before the earthquake sequence, due to slope instability in the eastern approach embankment: this was the cause of pre-existing cracks on the road pavement mainly above the embankment and at the embankment-abutment joint, but only marginally above the abutment.

Cracks were observed on the intrados of all the arches of the bridge, originating from the pier and propagating diagonally along the arch intrados. The widest cracks were found on the East arch, forming an X-shape pattern between the East abutment and mid-span (Figure 10e). This probably occurred due to the restraining effect of the East abutment against transverse displacement of the deck, which also caused horizontal cracking at the East arch springings at abutment and pier (Figure 10f and 10g).

The “Cinque Occhi” bridge (Figure 11) is located along the internal road connecting SS4 and SR260 routes, leading to Amatrice from the West. The bridge, which crosses over the Scandarello lake, consists of five arches (Figure 11a) for a total length of 60 m, supported by four tapered piers with rectangular cross-section and different heights. The bridge longitudinal axis is oriented along the NWW-SEE direction, which was subjected to higher PGA values during the August 24 event.

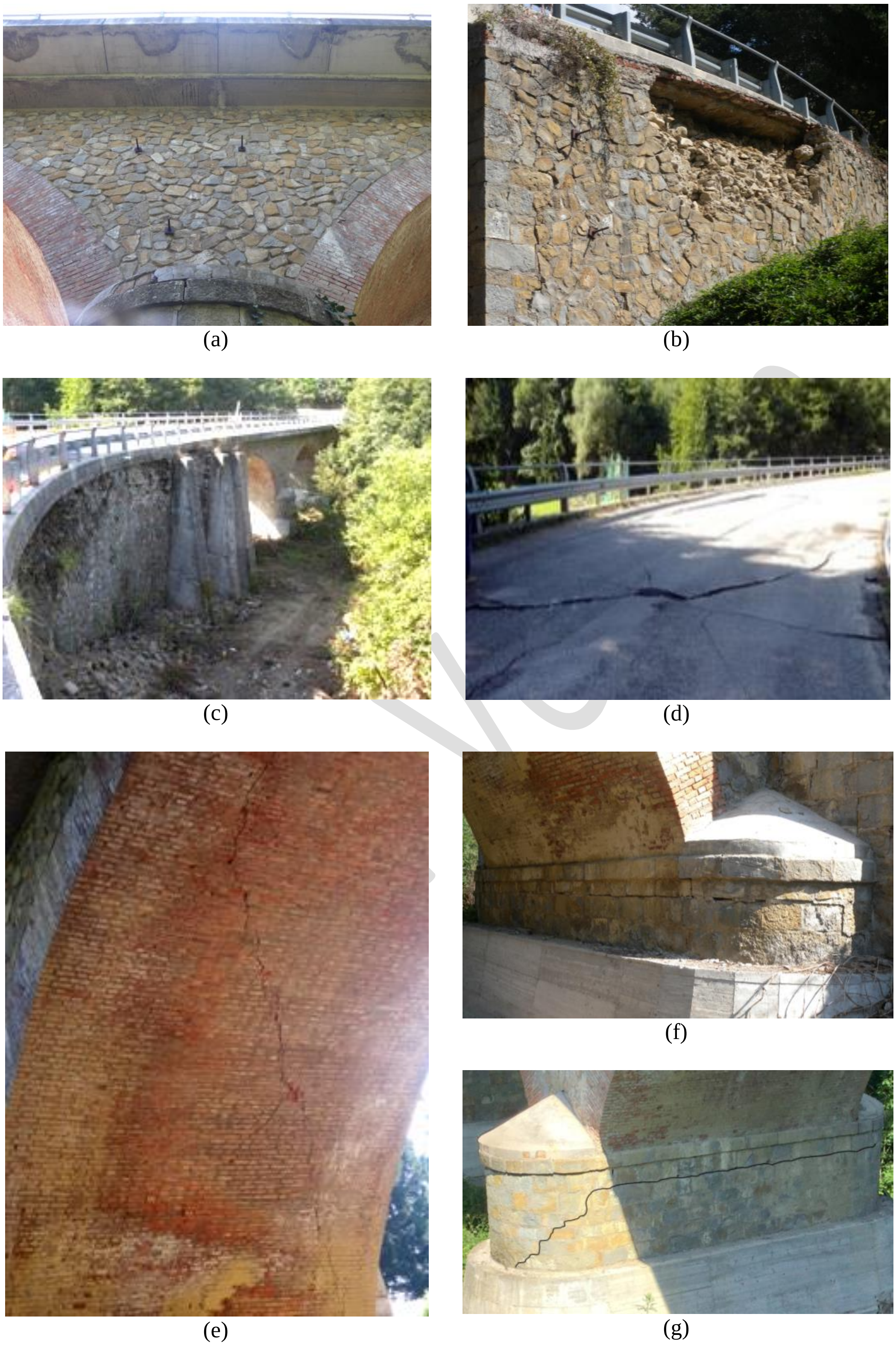

Figure 10 - “Tre Occhi” masonry bridge (42.620668 N, 13.290176 E): (a) partial collapse of the South-East wing wall; (b) buttresses and partial collapse of the North-East wing wall; (c) roadway settlement and cracks above the East abutment; (d) pre-existing cracks on the roadway at the East embankment-abutment joint (from Google Maps); (e) cracks on the East arch intrados; (f) cracks on the East arch springing at the abutment; (g) cracks on the East arch springing at the pier.

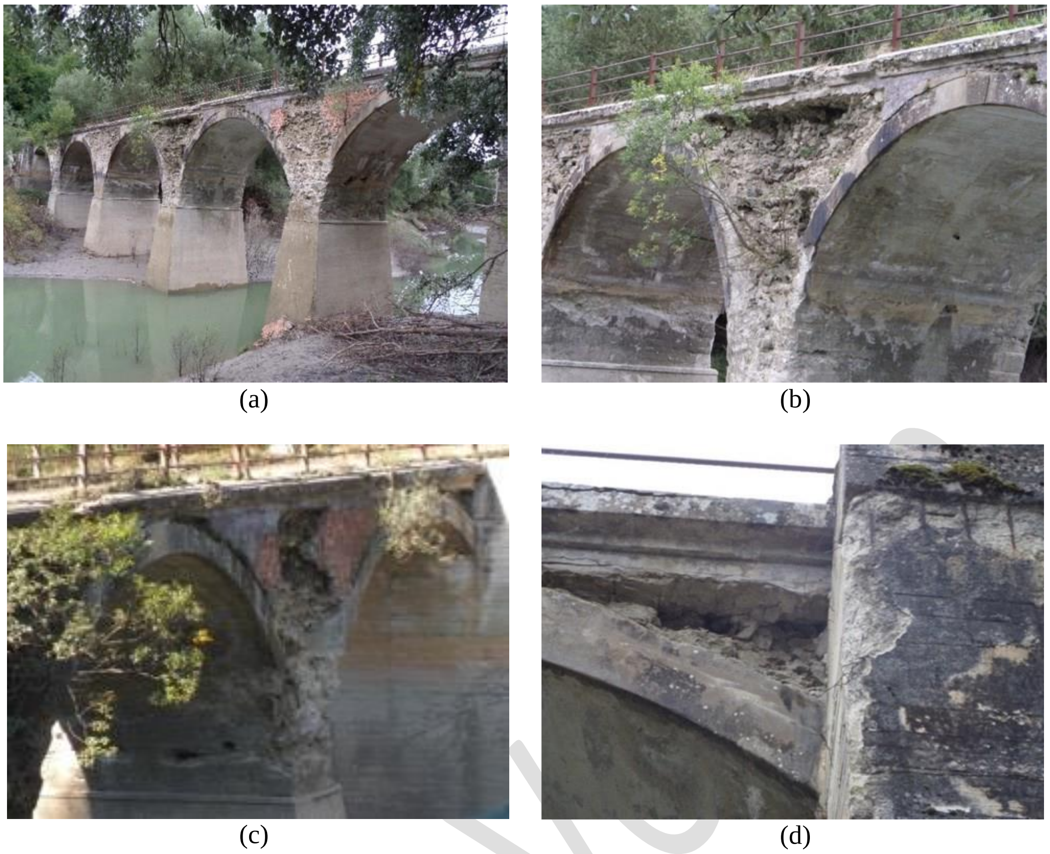

Figure 11 - “Cinque Occhi” masonry bridge (42.623178 N, 13.250428 E): (a) elevation view of the bridge; (b, c) partial collapse of masonry spandrel walls and loss of material at the arch springings, with evidence of previous retrofit and pre-existing damage; (d) collapse of a spandrel wall in proximity of the South abutment, with evidence of pre-existing damage to the reinforced concrete structure.

The masonry arrangement is similar to that of the “Tre Occhi” bridge, with original construction probably dating back to the beginning of the 20th century. The bridge was retrofitted with concrete jacketing of piers and arches intrados, while the original abutments were encased within reinforced concrete walls. Bridge maintenance was poor, leading to widespread pre-existing conditions (Figures 11b through 11d). In particular, a combination of damaged plaster and masonry with vegetation growth could be observed on the spandrels, while loss of material and exposure of steel reinforcement affected arches and abutments. The deck parapet appeared to be inadequate compared to current vehicle traffic.

The August 24 earthquake worsened the pre-existing damage pattern of the bridge, causing diffused out-of-plane failure of the spandrel walls (Figures 11a through 11d), due to low quality of the masonry and lack of ties. Localized losses of concrete cover and masonry units can be observed at the pier springing (Figures 9b and 11c): this can be associated with the development of horizontal hinges, as part of a longitudinal global mechanism facilitated by the pier slenderness and by the limited arch thickness-to-span ratio. Some damage was also observed on the spandrels close to the South abutment (Figure 11d). The bridge deck was not cracked along the roadway surface nor at the abutments: thus, structural safety was judged as not compromised by the earthquake and no traffic restrictions were applied.

Two arch bridges have been inspected along the “Trisungo-Tufo” road, in the locality of Tufo. The first one is a single-span arch stone masonry bridge (Figure 12), made with stone voussoirs of variable thickness. The bridge is oriented along the NEE-SWW direction, so it was subjected to higher PGA values along its longitudinal (partially inclined) direction. Cracks on the road surface over the abutments (Figure 12b) were caused by seismically induced infill settlements, related to displacements of the earth-retaining wing walls. Local cracking within load-bearing masonry elements, and spalling of the external leaf of the abutments and of the vault intrados (Figure 12c and 12d) were also observed.

Similar effects were observed for the second arch bridge along the “Trisungo-Tufo” route (Figure 13), a three-span arch structure made of stone masonry. The abutments and the piers are made of stone masonry, with an external leaf made of larger blocks, and an internal infill made of smaller stones, laid with mortar of poor characteristics and some loose material. This bridge has a curved longitudinal axis, with the mid-span radius oriented along the East-West direction, which was subjected to the highest PGA during all the main events.

In this case, out-of-plane overturning of the masonry parapets above the central span of the bridge occurred (Figure 13a and 13b). Moreover, the bridge comprises an older part and an adjacent relatively recent parallel extension; the latter behaved poorly during the earthquake, and experienced spalling of the external masonry leaf in the North abutment (Figure 13c) and cracks of one masonry pier (Figure 13d). These local effects were primarily due to the poor connection between the stone blocks, which led to loss not only of single units, but also of entire portions of the abutment walls. Horizontal cracks at the haunches can be compatible with an initial formation of plastic hinges.

Both the bridges in the locality of Tufo showed evidence of damage on the road surface (Figure 12b), as a result of abutment infill settlements. These effects induced local officials to limit traffic on the SP129 bridges.

(a) (b) (c) (d)

Figure 12 - Single-span masonry bridge along the “Trisungo-Tufo” route (42.735981 N, 13.254862 E): (a) view of the bridge; (b) damage on the road pavement; (c) spalling of the outer leaf of the abutment; (d) spalling of the intrados of the vault.

(a) (b) (c) (d)

Figure 13 - Three-span masonry bridge along the "Trisungo-Tufo" route (42.73538 N, 13.253655 E): (a, b) out-of-plane collapse of the parapet over the central arch; (c) spalling and (d) cracking of some masonry elements.

3.3 Reinforced concrete bridges

A number of RC bridges and viaducts were inspected in the aftermath of the earthquake. The structures inspected in the Amatrice area include the mixed RC/masonry "Rosa" bridge, in the town of Retrosi, and some viaducts of the SS685 and SS4 routes, with focus on the "Scandarello" viaduct. Overall, the outcome of this reconnaissance was satisfactory in that damage to the RC infrastructure network was found to be limited, confirming the impression that stiff (i.e. short period) rather than flexible bridges, were more heavily damaged during this event.

In general, although the extent of damage seen can vary from earthquake to earthquake, and even bridge to bridge, recurring damage patterns emerge when performing reconnaissance. While none of the bridges inspected raised major concerns, some of these types of damage were documented over the course of the inspection. Some examples are reported below, with reference to the structures assessed.

The "Rosa" bridge (Figure 14) is part of the local road that connects the SR577 route with the village of Retrosi, near Amatrice. The bridge consists of three tapered RC girders over five spans, with Gerber joints in the middle of the second and fourth spans. Four masonry piers with rectangular cross-section and rounded ends support the girders; the inner core of the piers is made of irregular cobbles and mortar, while the external leaf consists of clay brick masonry. The abutments also present an exterior clay brickwork. The girders are connected only by friction to piers and abutments, without any supporting or restraining device. The bridge longitudinal axis is oriented along the NNE-SSW direction, so the bridge was subjected to higher PGA values along its transverse direction.

As shown in Figure 14, the bridge was poorly maintained, with severe signs of degradation and pre-existing damage. In particular, the concrete girders showed widespread loss of concrete cover, steel reinforcement exposure and advanced corrosion (Figure 14a), especially at the Gerber beam joints (Figure 14b). Masonry piers showed degradation mainly related to erosion, loss of mortar joints, and vegetation growth (Figure 14c). In addition, the connections between parapets and deck were poorly designed: at some locations the parapet posts were torn from the deck (Figure 14d), probably after vehicle collision, and were precariously suspended.

(a) (b) (c) (d) (e) (f)

Figure 14 - “Rosa” reinforced concrete and masonry bridge (42.623178 N, 13.250428 E): (a) elevation view of the North-East bay; (b) degradation of the reinforced concrete Gerber girders; (c) degradation of the masonry piers; (d) pre-existing damage of a parapet connection to the deck; (e, f) cracking and partial collapse of the exterior brick leaf of the piers.

After the August 24 event traffic restrictions were imposed on the “Rosa” bridge, with maximum vehicle weight limited to 3.5 t; a Bailey bridge bypass was built for heavier traffic. The earthquake caused local damage to the substructures (Figures 14e and 14f), with vertical cracks at the top of the masonry piers starting from the external girder support and local collapse of the exterior brick leaf. The poor quality of the masonry, combined with the weakening of the shear-friction transfer between girders and piers due to material degradation and significant vertical earthquake accelerations, appear to be the main causes of the observed damage.

The SS685 and the SS4 are two important state roads. These roads run predominantly East-West and represent major connections between the two Italian coasts. In the surroundings of Amatrice, a number of RC viaducts are part of this network, and were therefore inspected during the reconnaissance trip. These viaducts were built in the 1970s and 1980s and were designed with little to no attention for seismic details. The typical configuration of the viaducts assessed is shown in Figure 15, with reference to SS685. These systems represent an interesting case study, in that they are potentially susceptible to several of the structural issues discussed earlier. However, little or no earthquake-induced damage was found in all inspected structures, as in the case of the “Scandarello” viaduct along SS4 (Figure 16) between Amatrice and Accumoli.

(a)

(b)

Figure 15 - Typical configuration of the viaducts investigated along SS685: (a) location 42.752002 N, 13.267902 E; (b) location 42.756556 N, 13.277111 E.

Figure 16 - “Scandarello” reinforced concrete viaduct (42.643309 N, 13.266802 E; adapted from [29]).

The structural systems are made of pre-cast (usually pre-stressed) concrete beams, connected to each other by a cast in place slab. The beams are simply supported atop unbolted laminated rubber bearings resting above large pier crossheads. It should be noted that these elements were not designed as seismic protection devices, but rather to resist gravity loads only and to accommodate small rotations and small displacements induced by thermal effects. Additionally, unbolted bearings rely on the friction between rubber pads and adjacent concrete to resist lateral loads: as discussed earlier, they tend to slide as soon as the applied lateral forces overcome their frictional strength.

It is evident that, in this configuration, the bridge deck is poorly restrained against differential movements with respect to the substructure (although shear keys are sometimes present at the bent caps, to prevent excessive transverse displacements). However, bearings appeared to be in good state in all inspected bridges and not to have displaced from their original position, as shown in Figure 17.

No relevant damage to the piers was observed in any of the inspected structures. Considering the average geometric properties of piers and superstructures of these viaducts, the period of vibration of the bridges can be estimated around 1.0 s. This can partially explain the limited damage observed, in that the peak horizontal acceleration demand induced by the seismic event was recorded for structural periods of about 0.25 s.

Even though no unseating was documented, some damage was observed due to excessive longitudinal displacements of the superstructure. These uncontrolled displacements often induced pounding effects which, in turn, caused damage (i.e. visible cracking and spalling) to elements such as bent-caps, transverse diaphragms, and abutments, as shown in Figure 18, sometimes worsening pre-existing damage due to material deterioration.

Figure 17 - Bearing pads of a viaduct invesitgated along SS685 (courtesy of Totaro).

(a) (b)

Figure 18 - (a) Damage to bent cap and transverse diaphragms along SS685 (42.756556 N, 13.277111 E); (b) Damage to an abutment along SS4 (42.699565 N, 13.251978 E; courtesy of Totaro).

4 CASE STUDIES OF DAMAGED BRIDGES

4.1 Masonry bridges: simplified analysis of arch bridges

Among several possible analysis methods [30, 31, 32, 33], a simplified approach based on limit analysis was chosen in order to assess the values of spectral acceleration, a^*_0, that trigger the longitudinal and transverse failure mechanisms discussed in Section 2.1. The procedure consists of an iterative application of the principle of virtual work (PVW) to estimate a load multiplier α_0 for the horizontal seismic load. The collapse-triggering acceleration, a^*_0, can then be obtained by multiplying the seismic load multiplier, α_0, by the gravity acceleration, g, and dividing it by the fraction of the structural mass participating in the kinematic mechanism, e^*, following the verification method proposed by the Italian Technical Standards for Constructions [34]:

$$a_0^* = \frac{\alpha_0 \sum_1^n P_i}{M^*} = \frac{\alpha_0 g}{e^*} \tag{1}$$

$$e^* = \frac{g M^*}{\sum_1^n P_i} \tag{2}$$

The participating mass M^* can be calculated as:

$$M^* = \frac{\left(\sum_1^n \Delta x_{Gi} P_i\right)^2}{g \sum_1^n \Delta x_{Gi}^2 P_i} \tag{3}$$

where:
P_i is the weight of the generic i^{th} block and/or infill section of the kinematic mechanism;
n is the number of blocks and infill sections;
Δx_{Gi} is the virtual horizontal displacements of the application point G_i of each weight P_i.
Taking into account the main geometrical features of the arch bridges only, it is possible to obtain directly the collapse-triggering acceleration a^*_0, as discussed by [16].
To carry out local strength verifications on the abutments (flexural collapse, AB_NM; and shear collapse, AB_S) and at the abutment-foundation interface (sliding, AB_SL; and overturning, AB_OV), linear static approaches were adopted for the analysis. The bending moment capacity of the abutment at the ultimate limit state, M_{Rd}, is calculated assuming a stress-block diagram in compression, neglecting the tensile strength of the masonry:

$$M_{Rd} = \left(\frac{l^2 t \sigma_0}{2}\right)\left(\frac{1-\sigma_0}{0.85\, f_d}\right) \tag{4}$$

where:
l is the length of the wall;
t is the thickness of the wall;
σ_0 is the mean compressive stress, referred to the gross cross-sectional area;
$f_d = f_k / \gamma_M$ is the design compressive strength of the masonry;
γ_M is taken as 1.0 in the assessment procedure.
The abutment shear strength, V_{Rd}, is evaluated as follows:

$$V_{Rd} = l' t f_{vd} \tag{5}$$

where:
l' is the length of the portion of the wall subjected to compression
$f_{vd} = f_{vk} / \gamma_M$ is the design shear strength of the masonry;
γ_M is taken as 1.0 in the assessment procedure.
The structural safety checks for sliding and overturning at the abutment-foundation interface are based on simple equilibrium. They take into account the unfavorable effects due to static and dynamic actions of the soil acting on the abutment wall, the horizontal inertia due to the seismic acceleration on the abutment/pier, and the horizontal component of the arch action. On the other hand, the favorable effects of the structural dead loads and of the weight of the soil are accounted for. For the sliding verification, the frictional strength, F_{Rd}, shall be evaluated as follows:

$$F_{Rd} = N_{Sd} \tan\delta \tag{6}$$

where:
N_{Sd} is the sum of the design values of the vertical actions;
δ is the friction angle on the foundation interface.
The strength values obtained from these capacity models can then be converted in terms of limit spectral accelerations, for easier comparison to the values of collapse-triggering accelerations of the main local and global mechanisms. Tables 2 through 5 list the limit acceleration values for the examined masonry arch bridges, for the various possible mechanisms. The assumptions on each bridge geometry and material properties are directly specified in the tables, where L represents the arch span, H its rise, and s its structural thickness. The acceleration demand is given by the PGA of the closer recording station, $a_g S$, divided by an assumed behavior factor $q = 2$.
The actual collapse mechanism of the “Tre Occhi” bridge was not correctly predicted with this method, considering simple in plane or out-of-plane collapse mechanisms. The mechanism predicted by the kinematic approach would be the transverse spandrel-wall overturning followed by an arch-pier longitudinal failure. In reality, however, the SW-T mechanism was prevented by transverse ties. Also the AP-L mechanism did not occur because a global transverse mechanism (AP-T) was triggered earlier, including overturning of the abutment retaining buttresses, transverse displacements of the East abutment and pier, and lateral shear deformations of the East arch, with diagonal cracks in the barrel vault. Possible causes of this behavior can be attributed to the quality of the masonry wing walls, to the curved geometry of the East abutment, and to pre-existing damage to the abutment structure, which cannot be easily included in a kinematic analysis. A more detailed FEM macro-model is presented in Section 4.2 to further investigate the behavior of this structure, which cannot be effectively captured by the simplified approach.
The damage observed on the “Cinque Occhi” bridge included the collapse of the spandrel external leaf, which is the most likely mechanism (SW-T) according to the simplified approach. In addition, the formation of hinges, with horizontal cracks at the arch springings, can be related to a longitudinal arch-pier mechanism (AP-L) that is also a possible mechanism according to the simplified analysis.

Table 2 – Simplified analysis of “Tre Occhi” bridge.

Br1_Tre Occhi Bridge		
Acceleration demand, $a_g S / q$	***Long. [g]***	***Transv. [g]***
AMT (24/08/2016)	0.435	0.190
AMT (30/10/2016)	0.133	0.100
Mechanism	***Estimated limit acceleration [g]***	
AP-L	a^*_{01}	0.278
AP-T	a^*_{02}	0.382
SW-T	a^*_{03}	0.025
A_L	a^*_{04}	0.427
AB_SL	a^*_{06}	1.559
AB_OV	a^*_{07}	0.248
AB_NM	a^*_{08}	0.108
AB_S	a^*_{09}	0.511
Note: q = 2; modeling assumptions: L = 12.00 m, H = 4.47 m, s/L = 0.08, f_d = 5.00 MPa.		

Table 3 – Simplified analysis of “Cinque Occhi” Bridge.

Br2_Cinque Occhi Bridge		
Acceleration demand, $a_g S / q$	***Long. [g]***	***Transv. [g]***
AMT (24/08/2016)	0.435	0.190
AMT (30/10/2016)	0.133	0.100
Mechanism	***Estimated limit acceleration [g]***	
AP-L	a^*_{01}	0.149
AP-T	a^*_{02}	0.444
SW-T	a^*_{03}	0.025
A-L	a^*_{04}	-
AB_SL	a^*_{06}	1.529
AB_OV	a^*_{07}	0.195
AB_NM	a^*_{08}	0.112
AB_S	a^*_{09}	0.4
Note: q = 2; modeling assumptions: L = 9.50 m, H = 4.60 m, s/L = 0.07, f_d = 5.00 MPa.		

For the single-span “Trisungo-Tufo” bridge, the weaker mechanism according to the simplified approach would be the spandrel wall transverse failure (SW-T). The local masonry spalling at various heights on the vault intrados, although not clearly related to the formation of hinges, may be compatible with an initial triggering of a local arch mechanism in the longitudinal direction (A-L), which the second possible mechanism according to this procedure.

For the three-span “Trisungo-Tufo” bridge, the first expected mechanism, according to the simplified approach, is the spandrel wall transverse failure (SW-T): consistently, the actual and most severe damage was the out-of-plane overturning of the masonry parapets. Horizontal cracks at the southern haunches are also visible: this damage is compatible with the initial formation of hinges and the triggering of a global longitudinal mechanism (AP-L), which is the second most likely mechanism identified by the simplified analysis.

Table 4 – Simplified analysis of “Trisungo-Tufo” single-span Bridge.

Br4_Trisungo-Tufo Bridge, single span		
Acceleration demand, $a_g S / q$	***Long. [g]***	***Transv. [g]***
AMT (24/08/2016)	0.435	0.190
T1214 (30/10/2016)	0.302	0.211
Mechanism	***Estimated limit acceleration [g]***	
AP-L	a^*_{01}	-
AP-T	a^*_{02}	-
SW-T	a^*_{03}	0.025
A-L	a^*_{04}	0.367
AB_SL	a^*_{06}	1.560
AB_OV	a^*_{07}	1.560
AB_NM	a^*_{08}	1.214
AB_S	a^*_{09}	1.530

Note: q = 2; modeling assumptions: L = 6.00 m, H = 3.00 m, s/L = 0.13, f_d = 5.00 MPa.

Table 5 – Simplified analysis of “Trisungo-Tufo” three span bridge.

Br5_Trisungo-Tufo Bridge, three spans		
Acceleration demand, $a_g S / q$	***Long. [g]***	***Transv. [g]***
AMT (24/08/2016)	0.190	0.435
T1214 (30/10/2016)	0.211	0.302
Mechanism	***Estimated limit acceleration [g]***	
AP-L	a^*_{01}	0.287
AP-T	a^*_{02}	0.611
SW-T	a^*_{03}	0.050
A-L	a^*_{04}	-
AB_SL	a^*_{06}	1.560
AB_OV	a^*_{07}	1.211
AB_NM	a^*_{08}	0.362
AB_S	a^*_{09}	1.200

Note: q = 2; modeling assumptions: L = 7.00 m, H = 2.50 m, s/L = 0.36, f_d = 5.00 MPa.

4.2 Masonry bridges: non-linear static finite element analysis

Further analyses have been carried out on a model of the “Tre Occhi” bridge to understand the actual transverse collapse mechanism, with the overturning of the abutment retaining buttresses, and diffused cracking of the East abutment, pier and span, as represented in Figure 19.

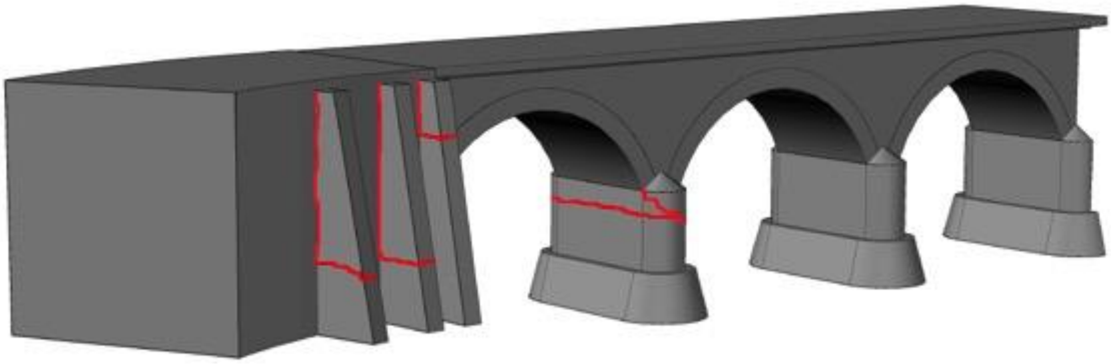

(a)

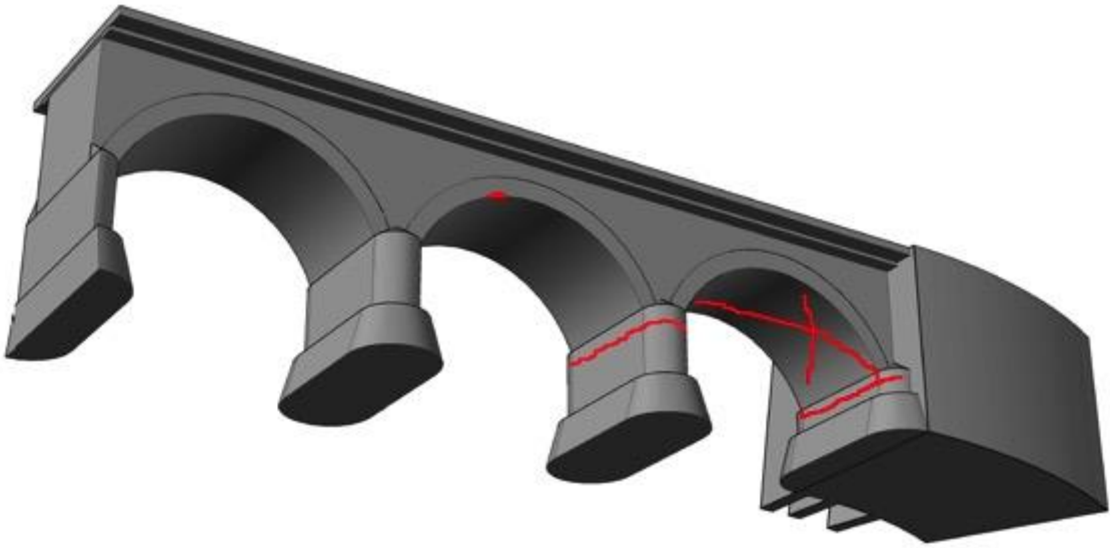

(b)

Figure 19 - Actual crack pattern of “Tre Occhi” bridge: views from (a) North and (b) South.

A macro-model consisting of 3D finite elements was developed using the FEM software TNO DIANA (Figure 20). The fill is included in the model employing elements with very low stiffness, in order to consider their contribution only to the translational mass, with a unit weight γ = 18 kN/m^3. Adequate boundary conditions are introduced to reproduce pier and abutment foundations. The “total strain crack” model is adopted to simulate the material behavior including softening, with parabolic behavior in compression and linear in tension. Masonry mechanical properties (elastic modulus E, Poisson’s ratio ν, compressive and tensile strengths f_c and f_t, and fracture energy parameters G_c and G_t) are summarized in Table 6.

On the basis of this preliminary model, non-linear static analyses were carried out considering separately the longitudinal and transverse direction. Capacity curves obtained in both cases are shown in Figure 21. The control point was chosen at the top of the central arch. The idealized elastic-perfectly plastic force-displacement relationship was determined according to the latest version of the Italian Technical Standards for Constructions [34].

Table 6 - Masonry properties.

γ [kN/m^3]	E [MPa]	ν [-]	f_c [MPa]	f_t [MPa]	G_c [N/mm]	G_t [N/mm]
18.00	900.00	0.20	5.00	0.20	5.00	0.0025

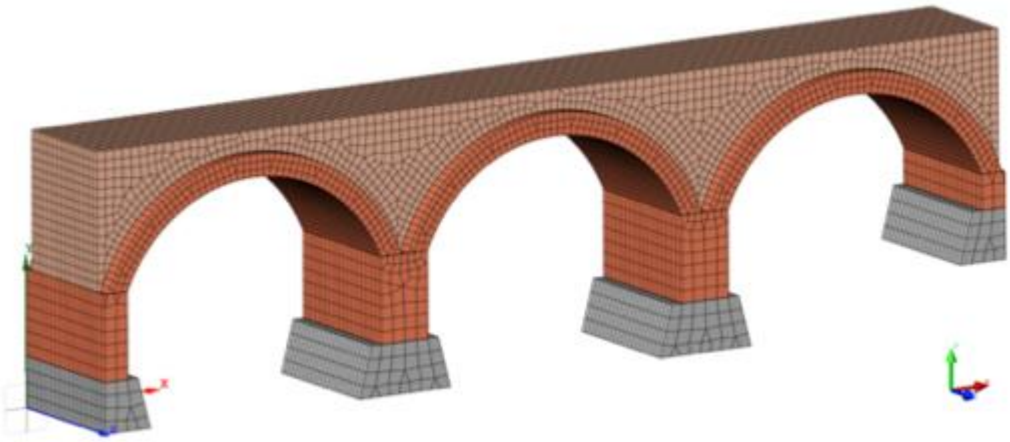

Figure 20 - “Tre Occhi” bridge 3D finite element macro-model.

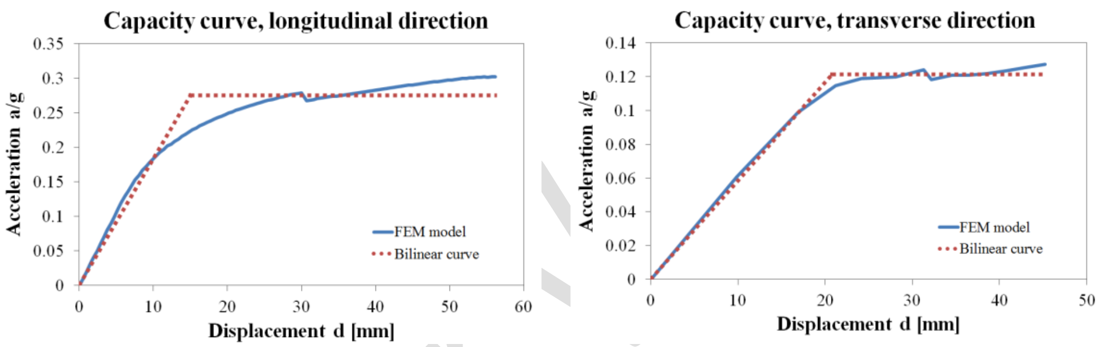

(a) (b)

Figure 21 - Capacity curve for (a) longitudinal and (b) transverse action.

The yielding acceleration of the bilinear relationship in the longitudinal direction is 0.275 g, which is consistent with the value of 0.278 g calculated according to the simplified method in Section 4.1, for the AP-L mechanism. In the transversal direction, however, the yielding acceleration is only 0.121 g, which is less than one third of the simplified result. This is consistent with what happened in reality, as a global transverse mechanism occurred and cracks related to longitudinal mechanisms have not been observed. Figure 22 shows the crack pattern obtained with non-linear static analysis in the transverse direction. It can be seen that the numerical crack pattern is fully compatible with the one observed after the earthquake, as shown in Figure 19.

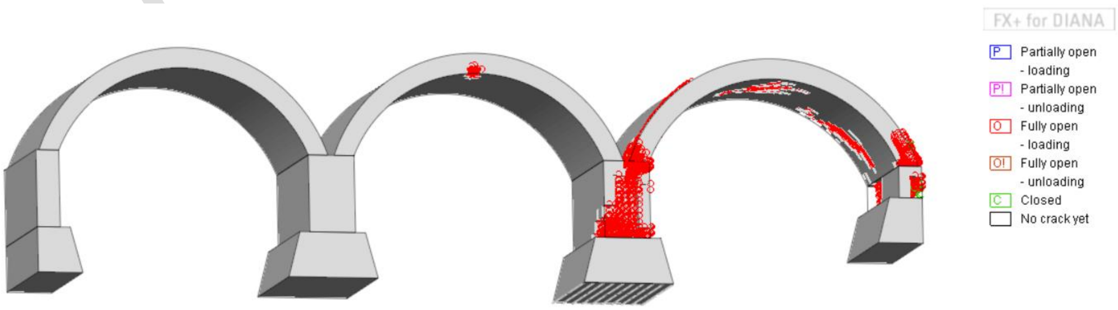

Figure 22 - Crack pattern predicted by the pushover analysis in the transverse direction.

4.3 Reinforced concrete bridges: linear static finite element analysis

The “Scandarello” viaduct along SS4 (Figure 16) was chosen as a case study and analyzed in more depth in this section, to provide deeper insight into the performance of the inspected RC bridges. More specifically, a linear 3D finite element model was used to obtain the dynamic properties of the bridge, and a response spectrum analysis was performed to obtain the seismic demand on the various structural elements, based on the spectrum from the August 24, 2016 event recorded in Amatrice.

The viaduct, presumably constructed in the late 1980s, is located in the municipality of Amatrice, in the Lazio region. It has a total length of 109 m, with five spans approximately 22-m long. Each span comprises nine precast, pre-stressed concrete beams, connected transversally via four RC diaphragms. The longitudinal beams are simply supported atop unbolted laminated rubber bearings, which sit on four large RC cap beams and two abutments. The cast in place RC deck is 11.5-m wide and is separated into five segments by means of six expansion joints.

Each of the four bents consists of two cast-in-place RC circular hollow-core columns, connected transversally at their top by a RC cap beam. The external diameter of all columns is 2.0 m at their base, while the columns height varies from 12 m to 13.7 m. Limited information is available on the cast-in-place RC abutments and on the pier foundations.

Except for this general information, some relevant data pertinent to the various structural elements are missing. Therefore, a number of geometric and material assumptions were necessary before the numerical model could be built:

- Columns: both external and internal diameter of all columns were assumed to be constant and equal to 2.0 m and 1.4 m, respectively;
- Cap beams: the RC cap beams were assumed to be 11.5-m long, with a 2.2-m x 1.5-m cross-section;
- Transverse diaphragms: the RC transverse diaphragms were assumed to be 10.5-m long, with a 0.25-m x 0.8-m cross section;
- Longitudinal beams: the 22-m long longitudinal beams were assigned the cross section properties of a “Type 60” State of Washington Bridge Girder (similar to a “Type III” AASHTO Bridge Girder), which is ideal for simply supported spans of about 20 m and is consistent with the cross section shape and dimensions that could be obtained from the available photographs of the case study bridge;
- Rubber bearings: the rubber bearings were assumed to be 0.46-m x 0.15-m pads, with a thickness of 0.04 m;
- Deck slab: the deck slab was assumed to be 0.25-m thick;
- Materials: (i) concrete was assigned an elastic modulus of 30,000 MPa, a shear modulus of 12,500 MPa and a unit weight of 25 kN/m^3; (ii) rubber was assigned an elastic modulus of 2.3 MPa and a shear modulus of 1.0 MPa.

The 3D linear elastic model of the viaduct, shown in Figure 23a, was built using the commercial software SAP2000 [35]. All beams and columns were modeled using elastic frame elements. These elements account for axial deformation, torsion, biaxial bending, and biaxial shear, as discussed by [36]. The pier foundations were assumed to provide full fixity at the base of the columns and were modeled accordingly. The abutments were modeled as simple supports instead. The deck slab provides in-plane diaphragm action with respect to longitudinal and transverse lateral loads, while offering limited contribution to resisting out-of-plane actions; for this reason, membrane elements were used to model the slab, as they transfer only in-plane forces. Each span was assigned an individual rigid diaphragm membrane [37], allowing relative motion between adjacent spans through expansion joints, especially in the transverse direction.

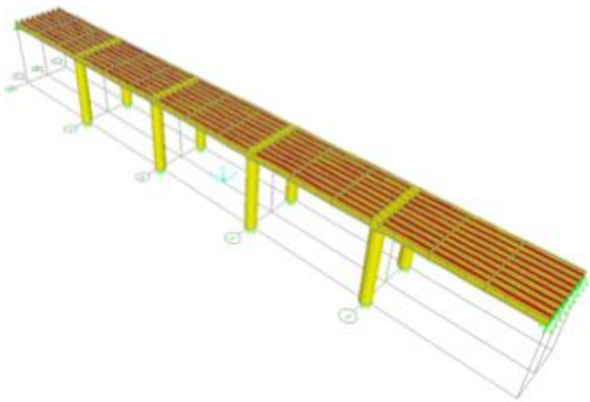

(a)

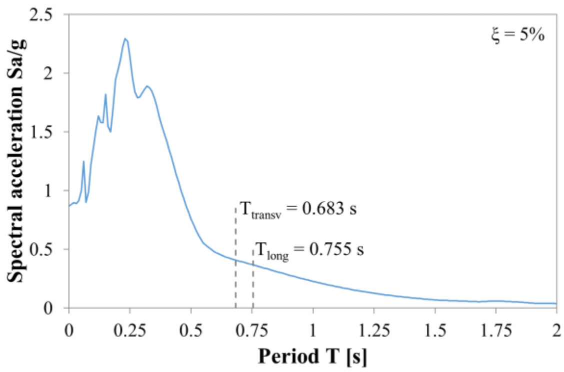

(b)

Figure 23 - “Scandarello” viaduct analysis: (a) 3D finite element model; (b) input response spectrum.

Bearings were introduced in the model by releasing the rotational degrees of freedom and by assigning partial fixity springs in the x, y and z directions, at the end of each longitudinal beam. The lateral stiffness (x and y direction) provided by the bearings was computed as *GA/h*, while the vertical stiffness (z direction) was computed as *EA/h*, where *G* and *E* are the shear modulus and the modulus of elasticity of rubber, *A* is the cross section of the bearing pads and *h* is the thickness of the bearings.

A weight per unit volume was assigned to the material specified for each element. Therefore, masses and weights were automatically accounted for in the model by the software.

The most relevant information extracted from the modal analysis of the bridge are its fundamental periods in the two major directions. The longitudinal fundamental period was estimated at 0.755 s, while the transverse fundamental period at 0.683 s. The seismic input employed to perform the response spectrum analysis was the acceleration response spectrum associated with the accelerograms recorded at the Amatrice Station (42.6325 N, 13.2866 E) on August 24, 2016, shown in Figure 23b. The two fundamental periods correspond to spectral accelerations of 0.363g and 0.403g in the longitudinal and transverse directions, respectively.

Previous earthquakes and simulations have shown that the seismic vulnerability of this kind of bridges is mainly related to the behavior of piers, bearings, and joints, while the response of the superstructure is of minor concern [37]. More specifically, columns may develop a ductile mechanism due to the formation of flexural plastic hinges, or a brittle flexural or shear failure, depending on the detailing quality. Thin unbolted rubber bearings may experience a slipping failure at the concrete-neoprene interface, which may result in large residual displacements, damage to bearings through tearing of rubber, unseating problems, and damage to beams and abutments due to pounding. Therefore, processing of the results of the response spectrum analysis was focused on the force and/or displacement demand on these elements.

Table 7 - Response spectrum analysis key results for the “Scandarello” viaduct.

Structural Element		Transverse direction			Longitudinal direction		
		M **[kNm]**	***V*** **[kN]**	***δ*** **[m]**	***M*** **[kNm]**	***V*** **[kN]**	***δ*** **[m]**
Column	Base	4649	1357	-	8375	1223	-
	Top	4649	1357	-	0	1223	-
Bearing		-	75	0.043	-	68	0.039

A single bent was analyzed under the longitudinal and lateral forces calculated from the spectral accelerations determined above. The entire translational mass tributary to the bent was considered effective as a first-mode mass in each direction. The columns were assumed to act as cantilevers in the longitudinal direction, while an inflection point was located at mid-height for response in the transverse direction. The key results of the analysis, for the most critical elements, are summarized in Table 7.

It is observed that the ground motion induces a shear force demand on columns and bearings about 10% higher when it acts in the transverse direction. This is due to the stiffer transverse response of the system, which attracts higher acceleration resulting in higher base-shear demand. However, it can be seen that the highest flexural demand is recorded at the base of the columns when the earthquake acts in the longitudinal direction. This is consistent with the boundary conditions of the piers, which rely on a frame mechanism in the transverse direction, and work as simple cantilevers with respect to longitudinal actions.

Because of the columns high slenderness, with an aspect ratio of about 6 when acting as cantilevers, it is reasonable to expect that a shear failure would be preceded by a flexural mechanism under longitudinal excitation. However, when the earthquake acts in the transverse direction, the column shear span is nearly halved, resulting in an aspect ratio of about 3 and in higher sensitivity to shear failure. To this end, the main concerns related to the performance of the columns of this bridge may be associated with their ability to sustain inelastic flexural deformations and to develop ductile plastic hinges in any direction, but also to resist high shear demands when subjected to transverse earthquake action.

Geometric data and material properties to evaluate precisely the strength and deformation capacity of the columns are not available. However, it is possible to estimate their flexural strength assuming an effective moment of inertia equal to half the gross-concrete section one, $I_{eff} = 0.5 \cdot I_g = 0.298$ m^4, a reinforcement yield strain $\varepsilon_y = 0.001$ (corresponding to a lower-bound yield stress of 215 MPa [38] and an elastic modulus of 210000 MPa), and a concrete elastic modulus $E_c = 30000$ MPa. Given the column outer diameter $D = 2$ m, the nominal yield curvature can be approximated as [39]:

$$\phi_y \approx 2.25 \frac{\varepsilon_y}{D} = 1.125 \cdot 10^{-3} \text{ rad/m} \tag{7}$$

The flexural strength is then estimated as:

$$M_{Rd} \approx E_c I_{eff} \phi_y = 10100 \text{ kNm} \tag{8}$$

which is larger than the elastic moment demands in both directions presented in Table 7. Similarly, the column shear strength can be roughly approximated assuming an effective shear area $A_{v,eff} = 0.8 \cdot A_g = 1.28$ m^2 [37], a concrete compressive strength $f_{ck} = 30$ MPa, and a reinforced concrete shear strength (including concrete and stirrup contributions):

$$f_{vd} \approx 0.33 \sqrt{f_{ck}} \big/ \gamma_M = 1.81 \text{ MPa} \tag{9}$$

where the partial coefficient $\gamma_M = 1.0$ for assessment. This results in the estimated shear strength:

$$V_{Rd} \approx f_{vd} A_{v,eff} = 2310 \text{ kN} \tag{10}$$

which also exceeds the computed shear demands. These approximate strength verifications are supported by the fact that no damage to the columns was documented.

At the bearing level, while unseating problems are most likely not to be expected, excessive displacements may result in pounding issues and in consequent damage of elements such as beams, diaphragms, deck slab, and abutments. At the same time, the displacement of the bearings may be of permanent nature, if the frictional strength of the elements is overcome by the lateral forces experienced during the seismic event and a slipping failure mode occurs. It is estimated that each bearing of the "Scandarello" viaduct carries an average weight of 187 kN. Assuming a rubber-to-concrete friction coefficient equal to 0.7 [40], the frictional strength of each bearing can be estimated as 131 kN, which is clearly higher than the demand from the analysis (75 kN). The maximum estimated bearing displacement was 0.043 m (Table 7), which corresponds to a shear strain of roughly 100%; this is lower than the deformation capacity of such bearings, since they can tolerate a shear strain of 150% without any sign of distress, while failure is typically associated to a shear strain of 300% [41]. Moreover, expansion joints allowed longitudinal displacements of at least 0.05 m before pounding, which are also larger than the calculated demand. These results provide numerical evidence in support of the reconnaissance observations, as no bearing slipping or pounding was observed.

It should be noted that the "Scandarello" viaduct did not experience any observable damage during the Central Italy Earthquake sequence and that the verifiable results of the analysis conducted are reasonably consistent with this field observation. However the results of this analysis can be considered of qualitative nature only, since accurate information about geometry and materials was missing and several assumptions were made to create the numerical model. Future studies supported by specific data may allow to estimate the capacity curves of the reinforced concrete elements and to perform a detailed non-linear analysis of the viaduct.

5 CONCLUSIVE REMARKS ABOUT LESSONS LEARNED FROM THE 2016 CENTRAL ITALY EARTHQUAKE FOR BRIDGES

5.1 Masonry bridges

The local road network in the surroundings of Amatrice was severely affected by damage to masonry bridges after the August 24, 2016 earthquake, causing traffic disruptions and requiring temporary replacements in two cases to restore emergency services. Considering the overall performance of masonry bridges in the aftermath of the 2016 Central Italy earthquake sequence, some general conclusions can be drawn:

- Masonry bridges in the area confirmed to possess a robust structural behavior, as overall structural safety was maintained by all examined structures.
- Local damage, disaggregation, and loss of masonry portions were observed in almost all of the structures, especially in spandrels, abutments, and piers. This damage was mainly due to the poor quality of materials and stone masonry arrangement, to the lack of maintenance, and to the deterioration of the structural elements.
- Out-of-plane overturning of the spandrel walls (SW-T) represents one of the most common collapse mechanism in all the analyzed bridges. This did not generally impaired the bridge structural safety, but in certain cases compromised its functionality and required traffic limitations. The addition of transverse steel tie-rods connecting the lateral spandrels proved its effectiveness in preventing this mechanism, as observed in the "Tre Occhi" bridge.
- The three bridges that were closed to traffic ("Tre Occhi" and both "Trisungo-Tufo" bridges) suffered damage to the abutment earth-retaining wing walls. Infill pressure and buttress ineffectiveness led to loss of support, that in the case of the "Tre Occhi" bridge triggered a global transverse mechanism (AP-T). Failure of these elements, which are often considered secondary for assessment purposes, can compromise not only the functionality, but also the overall stability of a bridge.

- Despite the lack of certain geometrical and mechanical data, the proposed simplified analyses could in general correctly predict the main failure mechanisms of the examined bridges. More refined analyses or a refinement of the proposed method are required to investigate the behavior of bridges characterized by special geometries or by the activation of mechanisms related to soil-structure interaction, as in the case of the "Tre Occhi" bridge.

5.2 Reinforced concrete bridges

Earthquake-induced damage to the RC infrastructure network was found to be limited, while extensive pre-existing conditions due to lack of maintenance and aging effects were reported. The reconnaissance activity can be summarized in the following conclusions:

- No serious damage to structural elements could be detected. Footings, columns, abutments, bearings, and superstructure generally appeared sound, except for pre-existing conditions related to poor maintenance.
- In some instances, minor damage caused by differential movements and excessive displacements of the superstructure was observed. These movements may have worsened the pre-existing conditions of some elements, for example causing spalling of previously deteriorated concrete.
- Some non-structural damage, for example to the bridge barriers, was also observed. In some cases, as for the barriers of the "Rosa" bridge near Amatrice, pre-existing non-structural damage may have been amplified by the earthquake shocks.
- A linear-elastic analysis was carried out on the "Scandarello" viaduct, a case-study representative of local reinforced concrete infrastructures. Despite the lack of information about geometric and mechanical properties, these preliminary results were aligned with the observed behavior, in that column and bearing capacities resulted larger than the estimated demands.

REFERENCES

[1] ReLUIS-INGV Workgroup (2016). Preliminary study on strong motion data of the 2016 central Italy seismic sequence V6. Available at http://www.reluis.it. Accessed on 12/07/2018.

[2] Stewart, J.P., Lanzo, G., Aversa, S., Bozzoni, F., Chiabrando, F., Grasso, N., Di Pietra, V., Dashti, S., Di Sarno, L., Durante, M.G., Foti, S., Franke, K., Reimschiissel, B., Galadini, F., Falcucci, E., Gori, S., Kayen, R.E., Mylonakis, G., Katsiveli, E., Pagliaroli, A., Giallini, S., Scasserra, G., Santucci de Magistris, F., Castiglia, M., Sica, S., Simonelli, A.L., Penna, A., Mucciacciaro, M., Silvestri, F., D'Onofrio, A., Chiaradonna, A., De Silva, F., Tommasi, P., Zimmaro, P. (2016). Engineering Reconnaissance Following the 2016 M6.0 Central Italy Earthquake: Ver 1. Report No. GEER-050A. Geotechnical Extreme Event Reconnaissance Association, University of California, Berkeley, CA, USA. DOI: 10.18118/G65K5W.

[3] Pinto, P.E., Mancini, G. (2009). Seismic assessment and retrofit of existing bridges. In: Manfredi, G., Dolce, M. (eds), The State of Earthquake Engineering Research in Italy: the ReLUIS-DPC 2005-2008 Project, pp. 111-140. Doppiavoce, Napoli, Italy. ISBN-13: 9788889972427.

[4] De Risi, R., Di Sarno, L. and Paolacci, F. (2017). Probabilistic seismic performance assessment of an existing RC bridge with portal-frame piers designed for gravity loads only. Engineering Structures, 145:348-367. DOI: 10.1016/j.engstruct.2017.04.053.

[5] Abbiati, G., Bursi, O.S., Caperan, P., Di Sarno, L., Molina, F.J., Paolacci, F., Pegon, P. (2015). Hybrid simulation of a multi-span RC viaduct with plain bars and sliding bearings. Earthquake Engineering and Structural Dynamics, 44(13):2221-2240. DOI: 10.1002/eqe.2580.

[6] Di Sarno, L., Del Vecchio, C., Maddaloni, G., Prota, A. (2017). Experimental response of an existing RC bridge with smooth bars and preliminary numerical simulations. Engineering Structures, 136:355-368. DOI: 10.1016/j.engstruct.2017.01.052.

[7] Kappos, A.J., Saiidi, M.S., Aydınoğlu, M.N., Isaković, T. (Eds.) (2012). Seismic Design and Assessment of Bridges - Inelastic Methods of Analysis and Case Studies. Springer, Netherlands. ISBN-13: 978-94-007-3943-7. DOI: 10.1007/978-94-007-3943-7.

[8] Del Vecchio, C., Kwon, O.S., Di Sarno, L., Prota, A. (2015). Accuracy of nonlinear static procedures for the seismic assessment of shear critical structures. Earthquake Engineering and Structural Dynamics, 44(10):1581-1600. DOI: 10.1002/eqe.2540.

[9] Di Sarno, L. (2013). Effects of multiple earthquakes on inelastic structural response. Engineering Structures, 56:673-681. DOI: 10.1016/j.engstruct.2013.05.041.

[10] Heyman, J. (1966). The stone skeleton. International Journal of Solids and Structures, 2(2):249-279. DOI: 10.1016/0020-7683(66)90018-7.

[11] Berger, E., Studer, J. (1981). Southern Italy Earthquake, November 23, 1980. Reconnaissance Summary. Earthquake Engineering Research Institute, Oakland, CA, USA.

[12] Han, Q., Du, X.L., Liu, J.B., Li, Z.X., Li, L.Y., Zhao J.F. (2009). Seismic damage of highway bridges during the 2008 Wenchuan earthquake. Earthquake Engineering and Engineering Vibration, 8(2):263-273. DOI: 10.1007/s11803-009-8162-0.

[13] Kawashima, K., Takahashi, Y., Ge, H., Wu, Z., Zhang, J. (2009). Reconnaissance report on damage of bridges in 2008 Wenchuan, China, earthquake. Journal of Earthquake Engineering, 13(7):965-996. DOI: 10.1080/13632460902859169.

[14] Earthquake Engineering Research Institute (2009). The Mw 6.3 Abruzzo, Italy, Earthquake of April 6, 2009. Available at https://www.eeri.org/site/images/eeri_newsletter/2009_pdf/LAquila-eq-report.pdf. Accessed on 12/07/2018.

[15] Clemente, P. (1998). Introduction to dynamics of stone arches. Earthquake Engineering and Structural Dynamics, 27(5):513-522. DOI: 10.1002/(SICI)1096-9845(199805)27:5<513::AID-EQE740>3.0.CO;2-O.

[16] da Porto F., Tecchio G., Zampieri P., Modena C., Prota A. (2016). Simplified seismic assessment of railway masonry arch bridges by limit analysis. Structure and Infrastructure Engineering, 12(5):567-591. DOI: 10.1080/15732479.2015.1031141.

[17] Tecchio, G., Donà, M., da Porto, F., (2016). Seismic fragility curves of as-built single-span masonry arch bridges. Bulletin of Earthquake Engineering, 14(11):3099-3124. DOI: 10.1007/s10518-016-9931-6.

[18] De Luca, A., Giordano, A., Mele, E. (2004). A simplified procedure for assessing the seismic capacity of masonry arches. Engineering Structures, 26(13):1915-1929. DOI: 10.1016/j.engstruct.2004.07.003.

[19] Resemini, S., Lagomarsino, S. (2004). Vulnerabilità sismica dei ponti ferroviari ad arco in muratura. Proc. of the 11th ANIDIS Conference "L'Ingegneria Sismica in Italia", pp. 25-29, Genova, Italy (in Italian).

[20] Singh, M.P., Khaleghi, B., Saraf, V.K., Jain, S.K., Norris, G (2002). Roads and Bridges. In: Jain, S.K., Lettis, W.R., Murty, C.V.R., Bardet, J.P. (eds), Bhuj, India Earthquake of January 26, 2001, Reconnaissance Report, pp. 363-379. Earthquake Spectra, supplement A to vol. 18. Earthquake Engineering Research Institute, Oakland, CA, USA.

[21] Cowan, M. (2011). R132 Kahu Road East-Bridge Status Summary Report. Available at http://resources.ccc.govt.nz/files/R132KahuRdEastBridge.pdf. Accessed on 12/01/2014.

[22] Zampieri, P., Tecchio, G., da Porto, F., Modena, C. (2015). Limit analysis of transverse seismic capacity of multi-span masonry arch bridges. Bulletin of Earthquake Engineering, 13(5):1557-1579. DOI: 10.1007/s10518-014-9664-3.

[23] Grossi, P., Williams, C., Cabrera, C., Tabucchi, T., Sarabandi, P., Rodriguez, A., Aslani H., Rahnama, M. (2011). The 2010 Maule, Chile earthquake: lessons and future challenges. Risk Management Solutions, Inc., Newark, CA, USA.

[24] Modena, C., Tecchio, G., Pellegrino, C., da Porto, F., Donà, M., Zampieri, P., Zanini, M. A. (2015). Reinforced concrete and masonry arch bridges in seismic areas: typical deficiencies and retrofitting strategies. Structure and Infrastructure Engineering, 11(4):415-442. DOI: 10.1080/15732479.2014.951859.

[25] Wang, P., Han, Q., Du, X. (2014). Seismic performance of circular RC bridge columns with flexure-torsion interaction. Soil Dynamics and Earthquake Engineering, 66:13-30. DOI: 10.1016/j.soildyn.2014.06.028.

[26] Kawashima, K., Aydan, O., Aoki, T., Kisimoto, I., Konagai, K., Matsui, T., Sakuta, J., Takahashi, N., Teodori, S., Yashima, A. (2010). Reconnaissance investigation on the damage of the 2009 L'Aquila, Central Italy earthquake. Journal of Earthquake Engineering, 14(6):817-841. DOI: 10.1080/13632460903584055.

[27] Ioannou, I., Borg, R., Novelli, V., Melo, J., Alexander, D., Kongar, I., Verrucci, E., Cahill, B., Rossetto, T. (2012). The 29th May 2012 Emilia Romagna Earthquake. EPICentre Field Observation Report No.EPI-FO-290512. UCL EPICentre, University College London, London, UK.

[28] Luzi, L., Puglia, R., Russo, E. & ORFEUS WG5 (2016). Engineering Strong Motion Database, version 1.0. National Institute for Geophysics and Volcanology, Observatories & Research Facilities for European Seismology, Italy. DOI: 10.13127/ESM".

[29] ANAS S.p.A., Condirezione Generale Tecnica Unità Ricerca e Innovazione (2010). Executive Technical Report, 04.11.2010 (in Italian).

[30] Brencich, A., De Francesco, U. (2004a). Assessment of multispan masonry arch bridges. I: Simplified approach. Journal of Bridge Engineering, 9(6):582-590. DOI: 10.1061/(ASCE)1084-0702(2004)9:6(582).

[31] Brencich, A., De Francesco, U. (2004b). Assessment of multispan masonry arch bridges. II: Examples and applications. Journal of Bridge Engineering, 9(6):591-598. DOI: 10.1061/(ASCE)1084-0702(2004)9:6(591).

[32] Galasco, A., Lagomarsino, S., Penna, A., Resemini, S. (2004). Non-linear seismic analysis of masonry structures. Proc. of the 13th World Conference on Earthquake Engineering, Vancouver, Canada.

[33] Rota, M., Pecker, A., Bolognini, D., Pinho, R. (2005). A methodology for seismic vulnerability of masonry arch bridge walls. Journal of Earthquake Engineering, 9(sup2):331-353. DOI: 10.1142/S1363246905002432.

[34] Ministry of Infrastructure (2008). Technical Standards for Constructions (DM 14.01.2008). Rome, Italy (in Italian).

[35] Computers and Structures, Inc. (2016). CSI Analysis Reference Manual For SAP2000, ETABS, SAFE and CSiBridge. ISO# GEN062708M1 Rev. 15. Berkeley, CA, USA.

[36] Bathe, K.J., Wilson, E.L. (1976). Numerical Methods in Finite Element Analysis. Prentice-Hall, Englewood Cliff, NJ, USA. ISBN-10: 0136271901 / ISBN-13: 9780136271901.

[37] Priestley, M.J.N., Seible, F., Calvi, G.M. (1996). Seismic Design and Retrofit of Bridges. John Wiley and Sons, New York, NY, USA. ISBN-10: 047157998X / ISBN-13: 9780471579984.

[38] Ministry of Public Works (1992). Technical Standards for the Construction of Reinforced and Prestressed Concrete and Steel Structures (DM 14.02.1992). Rome, Italy (in Italian).

[39] Priestley, M.J.N., Calvi, G.M., Kowalsky, M.J. (2007). Displacement-Based Seismic Design of Structures. IUSS Press, Pavia, Italy. ISBN-10: 8861980007 / ISBN-13: 9788861980006.

[40] Cardone, D., Perrone, G., Sofia, S. (2011). A performance-based adaptive methodology for the seismic evaluation of multi-span simply supported deck bridges. Bulletin Earthquake Engineering, 9(5):1463-1498. DOI: 10.1007/s10518-011-9260-8.

[41] Cardone, D. (2014). Displacement limits and performance displacement profiles in support of direct displacement-based seismic assessment of bridges. Earthquake Engineering and Structural Dynamics, 43(8):1239-1263. DOI: 10.1002/eqe.2396.